Journal of the Mechanics and Physics of Solids 59 (2011) 1966–1977

Contents lists available at ScienceDirect

Journal of the Mechanics and Physics of Solids

journal homepage: www.elsevier.com/locate/jmps

Theoretical analysis of electric, magnetic and magnetoelectric properties of nano-structured multiferroic composites

XiaoYan Lu [a], Hui Li [a], Biao Wang [b,*]

[a] School of Civil Engineering, Harbin Institute of Technology, Harbin 150001, China
[b] School of Physics and Engineering, Sun Yat-sen University, Guangzhou 510275, China.

ARTICLE INFO

Article history:
Received 23 November 2010
Received in revised form
20 June 2011
Accepted 23 July 2011
Available online 30 July 2011

Keywords:
Microstructures
Ferroelectric material
Energy method
Multiferroic composites

ABSTRACT

Electric, magnetic and magnetoelectric properties of the nano-structured multiferroic composites were studied by using an energy formulation with the consideration of the surface, interface, and size effect. Coupled thermodynamic evolution equations with respect to the spontaneous polarization and magnetization were established, in which the elastic fields in the matrix and inclusions were solved based on the Eshelby's equivalent inclusion concept and the Mori–Tanaka method. Physical properties of the composite, such as the spontaneous order parameters, piezoelectric/piezomagnetic properties, and the magnetoelectric coupling effect are highly dependent on the stress state and the microstructures of the nano-composites. Magnetoelectric coupling voltage coefficient was unstable in the vicinity of the critical size and disappeared below the critical size. The model is versatile enough for various composite structures.

1. Introduction

Multiferroic/magnetoelectric materials have drawn a continual interest because of the wide and potential applications such as the emerging field of spintronics, new data-storage media, multiple-state memories and sensors (Garcia et al., 2010; Nelson et al., 2010). In the past few years, great stride has been made both in single phase and in composite multiferroic materials. Since the single phase materials always showed weak magnetoelectric (ME) effect even in very low temperature, an alternative way to the commercial applications is to fabricate multiferroic composites composed of ferroelectric/piezoelectric (FE) and ferromagnetic/magnetostrictive (FM) phases. Multiferroic nano-heterostructures are keen of interest because of the large ME coupling effect in the room temperature and the small size for miniaturized multifunctional devices (Nan et al., 2008; Brintlinger et al., 2010).

The ME effect in multiferroic composites, either ceramic composites or nanostructures, are typically strain mediated and largely dependent on the efficiency of strain transferred across the interfaces separating the two components (Zheng et al., 2004). How to tailor and find an optimum stress states to induce the required interaction is crucial to reach large ME effect (MacManus-Driscoll et al., 2008; Lou et al., 2009). However, stress states in nano-heterostructures are complex because of the possible existence of the dislocations, coupling effects, different thermal expansion coefficients, and various defects. Besides, many factors, such as the lattice parameters of each part, substrate, elastic properties, electrostrictive and magnetostrictive properties can also greatly affect the stress state. Intensive experimental and theoretical studies have been focused on the strain-mediated nano-heterostructures. Although large ME coupling effect was gained in the room

* Corresponding author. Tel./fax: +86 20 84115692.
E-mail addresses: luxyhit@gmail.com (X. Lu), lihui@hit.edu.cn (H. Li), wangbiao@mail.sysu.edu.cn (B. Wang).

0022-5096/$ - see front matter © 2011 Elsevier Ltd. All rights reserved.
doi:10.1016/j.jmps.2011.07.007

temperature (Martin et al., 2010), the ME coupling effect is still much smaller than the theoretical predictions. This may suggest that there is a large room for the improvement of the material design and the fabrication, but reliable theoretical models are also needed.

In the past few years, a variety of models have been used, including the effective magnetoelectroelastic model to predict the effective constants of the composites at the linear stage and the phenomenological models to predict the behaviors at the nonlinear state. The magnetoelectric composites were first theoretically studied by Harshe et al. (1993a, 1993b) who obtained the expressions for the effective magnetoelectric coefficients. Later on, micromechanics models were used to estimate the effective properties of piezoelectric/piezomagnetic composite materials (Nan, 1994; Huang et al., 2009). By using the uniform field concept, exact connections between different components were obtained for the effective magnetoelectroelastic moduli of fibrous composite (Benveniste, 1995). Furthermore, Li and Dunn (1998) extended micromechanics approaches to analyze the average fields and effective moduli of heterogeneous media that exhibit full coupling between stationary elastic, electric, and magnetic fields. They also obtained the closed-form expressions for the effective moduli of fibrous and laminated composites (Li, 2000). The above models paid more attention on the effective properties of the composite. However, exact physical properties, which are the key features for use in functional devise were less concerned and not effectively investigated. Moreover, the linear constitutive equations with respect to the polarization, magnetization, and external fields are also not in accordance with the experimental results with nonlinear phenomenon (Slutsker et al., 2007). Using the micromechanics model together with the Landau free energy expansion, Lu et al. (2007) built a comprehensive model for 1–3 type composites. Critical behaviors were investigated for the Fe/FM multilayered system (Wang and Woo, 2008). Phase field models were also developed to predict the ME coupling in a nanocomposite thin film (Zhang et al., 2007a, 2007b; Wu et al., 2010). Analytical evolution fields of the spontaneous polarization, magnetization and stress were obtained with the use of a generalized Eshelby's equations and the Fourier transformation (Ni et al., 2010). However, the effect of the shape and size on the electric, magnetic and magnetoelectric coupling properties is still less concerned. Moreover, a more general thermomechanical model for composites with arbitrary-inclusions is of fundamental and technological interest.

In fact, the sets of the physical field equations of such heterogeneous magnetoelectroelastic solids under applied loadings are easy to set but not easy to be solved analytically because of the position-dependent constitutive coefficients (Ni et al., 2010). Thus, the estimates of the effective ME coefficients of the multiferroic composites were usually obtained by using various mean field approximations. The exact solutions for elastic homogeneous inclusion system, which are widely used in micromechanics analysis of heterogeneous materials are the well-known Eshelby's solutions because of the viability of the general ellipsoidal shape and the gentle and explicit solutions (Eshelby, 1957).

In this paper, the phenomenological theory combined with the Eshelby's inclusion theory was established to investigate the coupling effect and physical properties of nano-structured multiferroic composites. The stresses of the inclusions and matrix in the high temperature prototype were solved by using the classical elastic Eshelby's solutions. The time dependent order parameters can be derived by using the Ginzburg–Landau theory. Intrinsic properties of the composites including the phase transition temperatures, dielectric and piezoelectric properties of the FE phase, and piezomagneticity and the susceptibility of the FM phase were studied.

2. Coupled thermodynamic potential

Suppose that the FE thin film with imbedded FM inclusions was grown on a rigid substrate under high temperature. The film can be considered to be in-plane infinite and uniform in a large scale. In the fabrication temperature, above both the phase transition temperatures of the two phases, there is no phase transition occurs and this state is named as the prototype. FE phase transition and FM phase transition occurred when the temperature was cooled down to the room temperature. Correspondingly, FE transformation strain $\varepsilon_{ij}^{P}=Q_{ijkl}P_kP_l$ and FM phase transition strain $\varepsilon_{ij}^{M}=\lambda_{ijkl}M_kM_l/M_s^2$ were induced, with Q_{klij} the electrostrictive coefficient, P_k the spontaneous polarization vector, λ_{ijkl} the magnetostrictive coefficient, M_k the spontaneous magnetization vector, and M_s the saturation magnetization. Vigor's notation will be used in the following. Tensor suffix notation is bold-faced and used only where necessary. It should be noted that the thermal strain induced during the fabrication is ignored because of the small thermal difference among these two perovskite materials (Zheng et al., 2004).

Under applied initial strain induced by the substrate, the total free energy for the thin film can be written as the Gibbs free energy composing of the Landau free energy of the separated FE and FM composites, the coupling elastic energy, and the surface energy (Lu et al., 2009):

$$F=(1-f)\int_v F_L^E dv+f\int_v F_L^M dv+\int_v F_{Elas}dv+F_{Surf}, \tag{1}$$

where f is the volume fraction of the FM phase, F_L^E and F_L^M are the Landau-type bulk free energies of the FE and FM phases with the consideration of the gradient items induced by the inhomogeneous polarization and magnetization in the surface and interface. F_{Surf} is the total surface energy, and F_{Elas} is the elastic coupling energy.

2.1. Landau-type bulk free energy

For FE materials with a first order phase transition and FM materials with a second order phase transition, the bulk free energy densities for each phase are described by the conventional Landau-type expansions with polarization **P** and magnetization **M** served as the order parameters, respectively. It should be noted that the depolarization near the surface of the film is usually very important in nano-scale. However, proper boundary conditions can effectively suppress such effect (Woo and Zheng, 2008) in some structures such as the 1–3 type composites used in this work for simplicity.

In the absence of any applied field including electric, magnetic or mechanical fields, the polarization **P** is only induced by the spontaneous atomic displacements when going through a ferroelectric phase transformation. With the application of electric field **E** (including the external electric filed and depolarization field), another polarization $\mathbf{P}^{\mathrm{E}}$ is induced and can be linearly written as $\mathbf{P}^{\mathbf{E}}=\boldsymbol{\chi}_{\mathbf{b}}\mathbf{E}$, where χ_b is the background dielectric susceptibility and characteristic of the dielectric background materials. Thus, the electric displacement filed **D** at constant applied stress and temperature can be expressed in terms of the spontaneous polarization as (Zheng et al., 2010)

$$\mathbf{D}=\boldsymbol{\varepsilon}_0\mathbf{E}+\mathbf{P}+\mathbf{P}^{E}=\boldsymbol{\varepsilon}_0\mathbf{E}+\boldsymbol{\chi}_{\mathrm{b}}\mathbf{E}+\mathbf{P}=\boldsymbol{\varepsilon}\mathbf{E}+\mathbf{P}, \tag{2}$$

where ε_0 is the vacuum dielectric permittivity, ε is the total dielectric constant of the background material.

The thermodynamic potential without the surface energy can be obtained from the relation $dg_P/d\mathbf{E}=-\mathbf{D}=-\boldsymbol{\varepsilon}\mathbf{E}-\mathbf{P}$ with up to the 6th order Taylor expansions with respect to the spontaneous polarization $\mathbf{P}=(P_1,P_2,P_3)$ for the first order phase transition. Because of the existence of the inhomogeneous polarization, gradient items were also added. Under mechanical stress-free and electric-free boundary conditions, the total energy in the FE composite can be expressed as

$$\begin{aligned}F_L^E=&\,a_1(P_1^2+P_2^2+P_3^2)+a_{11}(P_1^4+P_2^4+P_3^4)+a_{12}(P_1^2P_2^2+P_1^2P_3^2+P_2^2P_3^2)\\&+a_{111}(P_1^6+P_2^6+P_3^6)+a_{112}[P_1^4(P_2^2+P_3^2)+P_2^4(P_1^2+P_3^2)+P_3^4(P_1^2+P_2^2)]\\&+a_{123}P_1^2P_2^2P_3^2+D_{11}^P(P_{1,1}^2+P_{2,2}^2+P_{3,3}^2)+D_{44}^P(P_{1,2}^2+P_{1,3}^2+P_{2,1}^2+P_{2,3}^2+P_{3,1}^2+P_{3,2}^2)\end{aligned} \tag{3}$$

where α_i,α_{ij} and α_{ijk} are the expansion coefficients of the Landau free energy. D_{11}^P and D_{44}^P are the corresponding gradient coefficients with the Voigt's notation.

Similar to the above description of dielectrics, the instant magnetostatic response of ferromagnetics is given by a constitutive relation $\mathbf{B}=\mu_0\mathbf{H}+\mathbf{M}^H+\mathbf{M}$, with **B** the magnetic induction, μ_0 the vacuum magnetic permeability, $\boldsymbol{M}^H$ the field induced effective magnetization, **H** the magnetic field, and **M** the spontaneous magnetization. It can also be written as the sum of the magnetic induction magnetization and the spontaneous magnetization. The magnetic induction **B** thus can be written as

$$\mathbf{B}=\mu_0\mathbf{H}+\boldsymbol{\mu}_{\mathrm{b}}\mathbf{H}+\mathbf{M}=\boldsymbol{\mu}H+\mathbf{M}, \tag{4}$$

where $\boldsymbol{\mu}_{\mathrm{b}}$ is the background magnetic susceptibility tensor and $\boldsymbol{\mu}$ is the total magnetic susceptibility tensor.

The thermodynamic potential for a bulk ferromagnetic material can be obtained from the relation $dg_m/d\boldsymbol{H}=-\boldsymbol{B}$. Since most common para-ferromagnetic phase transitions are a kind of the second order phase transition, the Taylor expansions of the thermodynamic potential can be expanded up to the 4th orders for the material in paramagnetic state with the cubic symmetry. With consideration of the magnetization gradients, the total energy potential without the surface energy can be written as

$$\begin{aligned}F_L^M=&\,\beta_1(M_1^2+M_2^2+M_3^2)+\beta_{11}(M_1^4+M_2^4+M_3^4)+\beta_{12}(M_1^2M_2^2+M_1^2M_3^2+M_2^2M_3^2)+D_{11}^M(M_{1,1}^2+M_{2,2}^2+M_{3,3}^2)\\&+D_{44}^M(M_{1,2}^2+M_{1,3}^2+M_{2,1}^2+M_{2,3}^2+M_{3,1}^2+M_{3,2}^2)\end{aligned} \tag{5}$$

where β_1 β_{11} and β_{12} are the thermal parameters for bulk FM material, D_{11}^M and D_{44}^M are the corresponding gradient coefficients.

2.2. Surface energy

The surface or interface eliminates all the symmetry elements, which change a vector perpendicular to the surface and generates a local field conjugated to the polarization component perpendicular to the surface (Bratkovsky and Levanyuk, 2005). The induced relaxation or restriction energy named as the surface energy F_{Surf} can be written as

$$F_{Surf}=\int_{s_P}\left(D_{11}^P\frac{P_i^2}{2\delta_i^P}+D_{44}^P\frac{P_i^2}{2\delta_j^P}\right)ds+\int_{s_M}\left(D_{11}^M\frac{M_i^2}{2\delta_i^M}+D_{44}^M\frac{M_i^2}{2\delta_j^M}\right)ds. \tag{6}$$

where s_P and s_M are the surface areas of the FE and FM phase, respectively. δ_i^P and δ_i^M $(i=1,2,3)$ are the extrapolation lengths for the FE and FM phases, respectively. We employ the usual suffix mutation. A repeated suffix is summed over the values 1, 2, 3 and suffixes preceded by a comma demote differentiation. The extrapolation lengths describe the difference of the surface and the bulk (Cottam et al., 1984; Qu et al., 1997).

2.3. Elastic interaction energy

Since the prototype in the high temperature has no phase transitions, the elastic fields both in the matrix and the inclusions can be solved by using the Eshelby's results without piezoelectric and piezomagnetic effects. When the temperature was cooled down below the phase transition temperatures, cubic to tetragonal phase transitions happen. The phase transition strains can be regarded as a pre-existed strain applied to the matrix and inclusion and affect the total energy of the system. The stable polarization and magnetization can be found when the total energy is the lowest.

Because of the lattice mismatch between the substrate and film, the specimen, which is clamped by the substrate, will be subjected to a uniform mismatch strains $\varepsilon^0=\varepsilon^0_{11}=\varepsilon^0_{22}$ during the fabrication process at high temperature (Lu et al., 2007). The elastic strains in the matrix and inclusions can be artificially derived by using Mori–Tanaka method (Benveniste, 1987), which can be divided into three steps: (i) In the high temperature, the average strain field in the matrix was changed with a perturbation strain ε' because of the distribution of the inclusions; (ii) When the temperature was cooled down below the FM phase transition temperature (phase transition temperatures of many FM materials are usually higher than those of common ferroelectric materials), FM phase transition occurred in the inclusion accompanying with a phase transition strain ε^M_{ij}. Together with the possible misfit strain ε^{PM}_{ij} induced by the difference of the lattices parameters of the two phases, the total induced eigenstrain in the inclusion can be written as $\varepsilon^{TI}_{ij}=\varepsilon^{PM}_{ij}+\varepsilon^M_{ij}$. In this state, the strain in the matrix was changed with another perturbation strain ε'' and was regarded as an average reference strain in the matrix; (iii) When the temperature was further cooled down below the FE phase transition temperature, FE phase transition ε^P_{ij} occurred and the average strain in the matrix which was regarded as a new average reference strain can be written as $\langle\varepsilon_{ij}\rangle=\varepsilon^0_{ij}+\varepsilon'_{ij}+\varepsilon''_{ij}-\varepsilon^P_{ij}$. The average strain in the inclusion thus can be derived based on the Mori–Tanaka method as (Mori and Tanaka, 1973)

$$\langle\varepsilon^I_{ij}\rangle=<\varepsilon_{ij}>+\tilde{\varepsilon}_{ij}-\varepsilon^{TI}_{ij}, \tag{7}$$

where $\tilde{\varepsilon}_{ij}$ is the strain corresponding to the stress disturbance.

Using the equivalent inclusion method, the stress of the inclusion has the following expression:

$$C^{\mathrm{I}}_{ijkl}[\langle\varepsilon_{kl}\rangle+\tilde{\varepsilon}_{kl}-\varepsilon^{\mathrm{TI}}_{kl}]=C^0_{ijkl}[<\varepsilon_{kl}>+\tilde{\varepsilon}_{kl}-\varepsilon^{\mathrm{TI}}_{kl}-\varepsilon^*_{kl}], \tag{8}$$

where C^I_{ijkl} and C^0_{ijkl} are elastic modulus tensors of the prototype FM inclusions and FE matrix, respectively. ε^*_{kl} is a fictitious strain, also named as equivalent eigenstrain, introduced for the calculation due to the different elastic moduli of the inclusion and the matrix. By far, the shape of the inclusion is arbitrary. Since the general ellipsoid is versatile enough to cover a wide variety of particle cases, we just focus on the ellipsoidal inclusion. In the initial state without external electric field and magnetic field, $\tilde{\varepsilon}_{ij}$ has the following relationship with the eigenstrains in the inclusion (Mura, 1987):

$$\tilde{\varepsilon}_{kl}=S_{klmn}(\varepsilon^{TI}_{mn}+\varepsilon^*_{mn}). \tag{9}$$

Thus, the average elastic strain in the inclusions can be rewritten as

$$\langle\varepsilon^{\mathrm{I}}_{kl}\rangle=<\varepsilon_{kl}>+S_{klmn}(\varepsilon^*_{mn}+\varepsilon^{TI}_{mn})-\varepsilon^{TI}_{kl}. \tag{10}$$

Since the prototype is the para-state with cubic symmetry, we adopted the Eshelby's tensor S_{klmn} for cubic anisotropy to calculate the initial disturbance strain without applications of external electric and magnetic fields. Based on the Mori–Tanaka theory, the strain equilibrium equation with the consideration of external substrate strain can be written as

$$f\langle\varepsilon^I_{kl}\rangle+(1-f)<\varepsilon_{kl}>=\varepsilon^0_{kl}. \tag{11}$$

By substituting Eq. (10) into Eq. (11), the average elastic strain in the matrix is

$$\langle\varepsilon_{kl}\rangle=\varepsilon^0_{kl}-fC^I_{klmn}(\tilde{\varepsilon}_{mn}-\varepsilon^{TI}_{mn}). \tag{12}$$

The fictitious strain ε^* finally can be found by substituting of Eqs. (10) and (12) into Eq. (8):

$$\boldsymbol{\varepsilon}^*=[\mathbf{C}^0-(1-c_f)(\mathbf{C}^0-\mathbf{C}^{\mathrm{I}})\mathbf{S}]^{-1}[(\mathbf{C}^0-\mathbf{C}^{\mathrm{I}})\boldsymbol{\varepsilon}^0+\mathbf{C}^{\mathrm{I}}\boldsymbol{\varepsilon}^{\mathrm{I}}]-\boldsymbol{\varepsilon}^{\mathrm{I}}\quad=\mathbf{A}\boldsymbol{\varepsilon}^0+\mathbf{B}\boldsymbol{\varepsilon}^{\mathrm{TI}}=\mathbf{A}\boldsymbol{\varepsilon}^0+\mathbf{B}(\boldsymbol{\varepsilon}^{PM}+\boldsymbol{\varepsilon}^M), \tag{13}$$

where

$$\begin{aligned}&\mathrm{A}=[\mathbf{C}^0-(1-f)(\mathbf{C}^0-\mathbf{C}^{\mathrm{I}})\mathbf{S}]^{-1}[(\mathbf{C}^0-\mathbf{C}^{\mathrm{I}}),\\&\mathrm{B}=[\mathbf{C}^0-(1-f)(\mathbf{C}^0-\mathbf{C}^{\mathrm{I}})\mathbf{S}]^{-1}\mathbf{C}^{\mathrm{I}}+\mathbf{I},\end{aligned} \tag{14}$$

with identity matrix $\mathbf{I}$. The fictitious strain is related with the spontaneous eigenstrain and the misfit strain induced by the lattice mismatch of the two phases or the thermal difference. In this work, the misfit strain is only taken into account.

Substitute Eqs. (13) and (14) back into Eqs. (10) and (12), the average elastic strain in the matrix and in the inclusion can be yielded as

$$\begin{aligned}&\langle\varepsilon_{ij}\rangle=(I_{ijkl}-fS_{ijmn}A_{mnkl})\varepsilon^0_{kl}-fS_{ijmn}(I_{mnkl}+B_{mnkl})\varepsilon^{TI}_{kl};\\&\langle\varepsilon^I_{ij}\rangle=[I_{ijkl}-A_{ijkl}+(1-f)S_{ijmn}A_{mnkl}]\varepsilon^0_{kl}+[(1-f)S_{ijmn}-I_{ijmn}](I_{mnkl}+B_{mnkl})\varepsilon^{TI}_{kl}.\end{aligned} \tag{15}$$

The corresponding elastic stresses are $\langle \sigma_{ij} \rangle = C^0_{ijkl} \langle \varepsilon_{kl} \rangle$ and $\langle \sigma^I_{ij} \rangle = C^I_{ijkl} \langle \varepsilon^I_{kl} \rangle$ in the matrix and inclusions, respectively. They are both functions of the order parameters.

The total coupled elastic energy density F_{Elas} can be finally calculated by combining the elastic energy in each composite:

$$F_{Elas} = \tfrac{1}{2} f \langle \sigma^I_{ij} \rangle \langle \varepsilon^I_{ij} \rangle + (1-f) \langle \sigma_{ij} \rangle \langle \varepsilon_{ij} \rangle. \tag{16}$$

3. Physical properties of 1–3 type multiferroic heterostructures

1–3 Type multiferroic thin film with the FM pillars ($CoFe_2O_4$) embedded in the FE matrix ($BaTiO_3$) grown on a rigid substrate $SrTiO_3$ has a good connectivity and large contact areas (Zavaliche et al., 2007). $BaTiO_3$ is cubic in the paraelectric phase and undergoes a cubic to tetragonal phase transition when the temperature is down below the critical phase transition temperature. The ease direction of the polarization will be along the direction in which $BaTiO_3$ is under stretch, and/or vertical to the direction in which $BaTiO_3$ is under constraint. $CoFe_2O_4$ is unique among ferrites because of its high values of magneto-crystalline anisotropy and magnetostriction (Chambers et al., 2002). Most importantly, the lattice parameter is half-comparable with that of $BaTiO_3$. In the highly strained structure, the nano-pillars under constraint will have ease axis along the vertical direction (Brown et al., 2001). It was assumed that the direction of the single domain magnetic component is perpendicular to the interface of the film/substrate. The depolarization field may be great in a thin film, but weak in cylinders, especially in the slim cylinders. For simplicity, the condition $P_3 = P \neq 0, P_1 = P_2 = 0$ and $M_3 = M \neq 0, M_1 = M_2 = 0$ without the depolarization field is first considered.

Both theories and experiments have shown that the in-plane strain distribution is not uniform because of the large mismatch in the FE/FM interface (Zhang et al., 2007a, 2007b). The order parameters are both functions of x and z. The Landau free energy for a cubic FE and FM materials thus can be simplified as (Lu et al., 2007)

$$F^E_l = (1-f) \int_v \left[\alpha_1 P + \alpha_{11} P^3 + \alpha_{111} P^5 + D^P_{11} \left(\frac{\partial P}{\partial z} \right)^2 + D^P_{44} \left(\frac{\partial P}{\partial x} \right)^2 \right] dv, \tag{17}$$

$$F^M_l = f \int_v \left[\beta_1 M^2 + \beta_{11} M^4 + D^M_{11} \left(\frac{\partial M}{\partial z} \right)^2 + D^M_{44} \left(\frac{\partial M}{\partial x} \right)^2 \right] dv. \tag{18}$$

In the same way, the surface energy can be written as

$$F_{surf} = (1-f) \left(D^P_{11} \int_s \frac{P^2}{\delta^P_3} ds + D^P_{44} \int_s \frac{P^2}{\delta^P_1} ds \right) + f \left(D^M_{44} \int_s \frac{M^2}{\delta^M_3} ds + D^M_{11} \int_s \frac{M^2}{\delta^M_1} ds \right). \tag{19}$$

Since the composite film is expitaxially grown on a rigid substrate, there is an elastic strain induced by the substrate which is noted as ε^0. In fact, ε^0 is relative with the volume fractions of each part and the lattice mismatch of each phase with the substrate. Here we just use a series of average value to investigate the substrate effect.

With the average initial strain ε^0_{ij} and total eigenstrain of the inclusion ε^{TI}_{kl}, the coupling elastic energy F_{Elas} can be derived by using Eqs. (15) and (16) with the Eshelby's tensor components for infinitely long cylindrical inclusions with cubic symmetry (Mura, 1987).

3.1. Time dependent Ginzburg–Landau equations

The temporal evolution of the polarization and magnetization fields can be derived by approaching the total free energy at a rate proportional to the consequent free energy change (Lu et al., 2009)

$$\frac{\partial P(x,z,t)}{\partial t} = -L^E (1-f) \left[\alpha^*_1 P + \alpha^*_{11} P^3 + 6\alpha_{111} P^5 - D^P_{11} \frac{\partial^2 P}{\partial z^2} - D^P_{44} \frac{\partial^2 P}{\partial x^2} \right], \tag{20}$$

$$\frac{\partial M(x,z,t)}{\partial t} = -L^M f \left[2\beta^*_1 M + 4\beta^*_{11} M^3 - D^M_{11} \left(\frac{\partial^2 M}{\partial z^2} \right) - D^M_{44} \left(\frac{\partial^2 M}{\partial x^2} \right) \right], \tag{21}$$

with normalized coefficients

$$\begin{aligned} &\alpha^*_1 = 2\alpha_1 + A^P_{Elas}, \quad \alpha^*_{11} = 4\alpha_{11} + B^P_{Elas}, \\ &\beta^*_1 = 2\beta_1 + A^M_{Elas}, \quad \beta^*_{11} = 4\beta_{11} + B^M_{Elas}, \end{aligned} \tag{22}$$

where L^E and L^M are the kinetic coefficients concerning the domain wall mobility. A^P_{Elas}, B^P_{Elas} and A^M_{Elas}, B^M_{Elas} are the linear and nonlinear coefficients of variations of the elastic coupling energy with respect to the polarization and magnetization order parameters, respectively. $\alpha_1 = A^P(T - T^P_{c0})$ and $\beta_1 = A^M(T - T^M_{c0})$.

The corresponding boundary conditions can be expressed as

$$\frac{\partial P}{\partial z} = \mp \frac{P}{\delta_3^P}\left(z = \pm \frac{h}{2}\right); \quad \frac{\partial P}{\partial x} = -\frac{P}{\delta_1^P}(x = l_P), \ \frac{\partial P}{\partial n} = 0, \ (x = 0);$$
$$\frac{\partial M}{\partial z} = \mp \frac{M}{\delta_3^M}\left(z = \pm \frac{h}{2}\right); \quad \frac{\partial M}{\partial x} = -\frac{M}{\delta_1^M}(x = l_M), \ \frac{\partial M}{\partial n} = 0, \ (x = 0), \tag{23}$$

where $l_p = (1-\sqrt{f})l$ and $l_m = \sqrt{f}l$ with the considering element length l of the sample, and h is the thickness of the film.

The spontaneous polarization and magnetization are coupled together through the elastic interaction. The energy minimizing fields served as a result of artificial relaxation process and the steady solutions are the values of the average order parameters satisfying the conditions that the energy functional is stationary (Ni et al., 2010). We use the finite difference method to solve the time and spatial differential equations. In each time step, the average polarization and magnetization were calculated and substituted into the stress formulas for those of the next time step. The spontaneous polarization and magnetization can be found in the stable state of the coupling equations.

3.2. Linear analysis and phase transition temperatures

Critical temperature, which can be tuned by external strains plays a vital role in the appearances of many physical properties of the FE and FM materials. The polarizations can be unstable in the vicinity of the critical temperatures and disappears below the critical temperatures. The critical conditions of the dynamic stability can be studied through a bifurcation analysis of the nonlinear equations (Wang and Woo, 2009). We should note that the appearance of physical properties of ferroic materials have a direct relation with the critical properties. Based on the linear analysis theory (Wang and Woo, 2009), we apply infinitesimal perturbations Δ_P andΔ_M to the trivial stationary solutions $P_0=0$ and $M_0=0$. Neglecting the small higher order terms, Eqs. (20) and (21) become

$$\frac{\partial \Delta_P}{\partial t} = -L^E(1-f)\left(\alpha_1^* \Delta_P - D_{11}^P \frac{\partial^2 \Delta_P}{\partial z^2} - 2D_{44}^P \frac{\partial^2 \Delta_P}{\partial x^2}\right), \tag{24}$$

$$\frac{\partial \Delta_M}{\partial t} = -L^M f\left(\beta_1^* \Delta_M - D_{11}^M \frac{\partial^2 \Delta_M}{\partial z^2} - 2D_{44}^M \frac{\partial^2 \Delta_M}{\partial x^2}\right). \tag{25}$$

By separating variables and applying the boundary conditions, the phase para-ferro transition temperatures can be finally found as follows:

$$T_c^P = T_{c0}^P - \frac{1}{A^E}(D_{11}^P k_{Pz}^2 + 2D_{44}^P k_{Px}^2 - A_{Elas}^P),$$
$$T_c^M = T_{c0}^M - \frac{1}{A^M}(D_{11}^M k_{Mz}^2 + 2D_{44}^M k_{Mx}^2 - A_{Elas}^M). \tag{26}$$

The smallest values of k_{Pz},k_{Px},k_{Mz},k_{Mx} can be found from the boundary conditions. Substituting these results into Eqs. (26), we can obtain the critical temperatures for the phase transitions.

3.3. Stationary physical properties

With the average polarization $\langle P\rangle = \int_v P dv/v$, the dielectric and piezoelectric coefficients can be calculated based on the thermal relations by using the following equations:

$$\varepsilon_{33}^{P*} = {\varepsilon_0}^{-1}\left(\frac{\partial^2 F_{tot}}{\partial P^2}\right)^{-1} \approx {\varepsilon_0}^{-1}(\alpha_1^* \langle P\rangle + 3\alpha_{11}^* \langle P\rangle^2 + 5\alpha_{111}\langle P\rangle^4)^{-1}; \tag{27}$$

$$d_{33}^{P*} = 2Q_{11}\langle P\rangle \varepsilon_{33}^{P*}, \quad d_{31}^{p*} = 2Q_{12}\langle P\rangle \varepsilon_{33}^{P*}. \tag{28}$$

In the same way, with average magnetization $\langle M\rangle = \int_v M dv/v$, the susceptibility and piezomagnetization coefficients can be written as

$$\mu_{33}^{M*} = {\mu_0}^{-1}\left(\frac{\partial^2 F_{tot}}{\partial M^2}\right)^{-1} \approx {\mu_0}^{-1}(\beta_1^* \langle M\rangle + 3\beta_{11}^* \langle M\rangle^2)^{-1}, \tag{29}$$

$$q_{33}^{M*} = 2\lambda_{11}\langle M\rangle \mu_{33}^{M*}, \quad q_{31}^{M*} = 2\lambda_{12}\langle M\rangle \mu_{33}^{M*}. \tag{30}$$

3.4. Magnetoelectric coupling coefficients

Assuming that the two phases are perfectly bonded with ideal interface coupling, the linear magnetoelectric coupling coefficient can be derived by using an averaging method based on the constitutive equations. With the mechanical boundary condition $(1-f)\varepsilon_{ii}^{P}-f\varepsilon_{ii}^{M}=0$ $(i=1,2)$ and the electric open-circuit condition of $D_3=0$, the classical longitudinal magnetoelectric voltage coefficient for 1–3 type is (Liu et al., 2006)

$$\alpha'_{E,33}=\frac{-2f(1-f)d_{31}^{P*}q_{31}^{M*}}{[(s_{11}^{M}+s_{12}^{M})(1-f)+(s_{11}^{P}+s_{12}^{P})f^2/(1-f)]\varepsilon_{33}^{P*}-2(d_{31}^{P*})^2f^2/(1-f)}, \tag{31}$$

where s_{ij}^{P} and s_{ij}^{M} are the compliances of the FE and FM phases, respectively. q_{ij}^{M*} is the modified piezomagnetic coefficient. d_{ij}^{P*} and ε_{ij}^{P*} are the modified piezoelectric coefficient and permittivity of the ultra-thin film, respectively.

4. Results and discussions

The parameters taken from Liu et al. (2006, 2007) and the Eshelby tensor calculated for the cylindrical inclusion in $BaTiO_3$ cubic matrix were listed in Table 1. Because of the limited experimental data, gradient coefficients D_{11}^{M} and D_{44}^{M} were given with considerable values. The value of the extrapolation lengths are usually about 5–45 nm for $BaTiO_3$ and 43 nm is used here for the two phases, which may add some discrepancies especially when the volume fraction of portion is very small. The details for the calculation of the Eshelby tensor for cubic symmetry crystals with column shape are listed in Appendix A.

The length of one element l was taken as 100 nm and the thickness of the film is set as 2000 nm, which can be approximately regarded as infinite compare with the length of the composites. $CoFe_2O_4$ has a maximum magnetostriction of about -590 ppm in (100) direction and an opposite value of about 120 ppm in the (111) direction. Since there is no exact expression of the eigenstrain for materials with large magnetostriction, we set $\lambda_{11}=-590$ ppm and $\lambda_{12}=\lambda_{13}=120$ ppm for a glance.

As shown in Fig. 1, external compressive strain can enhance the critical temperature of the FE phase, but acts in an opposite way to that of the FM phase. The difference can be illustrated by the stress effect on the physical properties of the crystals. For $BaTiO_3$, an in-plane constraint or vertical tensile strain can enhance the polarization along the vertical direction. While for $CoFe_2O_4$ with negative magnetostriction in the (001) direction, a tensile in-plane strain and compressive vertical strain can

Table 1
Parameters of the FE and FM phases.

$BaTiO_3$	$CoFe_2O_4$
$C_{11}^{0}=C_{22}^{0}=C_{33}^{0}=1.76\times10^{11}N/m^2$, $C_{12}^{0}=C_{13}^{0}=C_{23}^{0}=0.846\times10^{11}N/m^2$, $C_{44}^{0}=C_{55}^{0}=C_{66}^{0}=0.43\times10^{11}N/m^2$ $Q_{11}=0.11\,m^4/C^2$, $Q_{12}=-0.043\,m^4/C^2$. $a_p=0.3994\times10^{-9}$ m $A^P=3.3\times10^5\,m/FK$, $T_{c0}^{P}=383$ K, $\alpha_{11}=3.6\times10^6\times(T-448.15)\,m^5/C^2F$, $\alpha_{111}=6.6\times10^9\,m^9/C^4F$, $D_{11}^{P}=2.7\times10^{-9}$, $D_{44}^{P}=0.45\times10^{-9}\,m^3/F$, $\delta_1^{P}=\delta_3^{P}=43\times10^{-9}$ m.	$C_{11}^{1}=C_{22}^{1}=C_{33}^{1}=2.86\times10^{11}N/m^2$ $C_{12}^{1}=C_{13}^{1}=C_{23}^{1}=1.73\times10^{11}N/m^2$ $C_{44}^{1}=C_{55}^{1}=C_{66}^{1}=0.453\times10^{11}N/m^2$ $\lambda_{11}=-590\times10^{-6}$, $\lambda_{12}=\lambda_{13}=120\times10^{-6}$ $a_m=0.838\times10^{-9}$ m, $\tilde{a}_m=0.419\times10^{-9}$ m, $M_s=300\times10^3\,A/m$, $T_{c0}^{M}=793$ K, $A^M=9.5\times10^3$, $\beta_{11}=3.75\times10^6$, $D_{11}^{M}=72\times10^{-16}$, $D_{44}^{M}=36\times10^{-16}\,Jm/A^2$, $\delta_1^{M}=\delta_3^{M}=43\times10^{-9}$ m.
$S_{11}=S_{22}=0.6899$, $S_{12}=S_{21}=0.0561$, $S_{31}=S_{32}=0.2423$, $S_{55}=0.4998$, $S_{66}=0.3097$, $S_{44}=0$, $S_{13}=S_{23}=S_{33}=0$. $a_s=0.3905\times10^{-9}$ m	

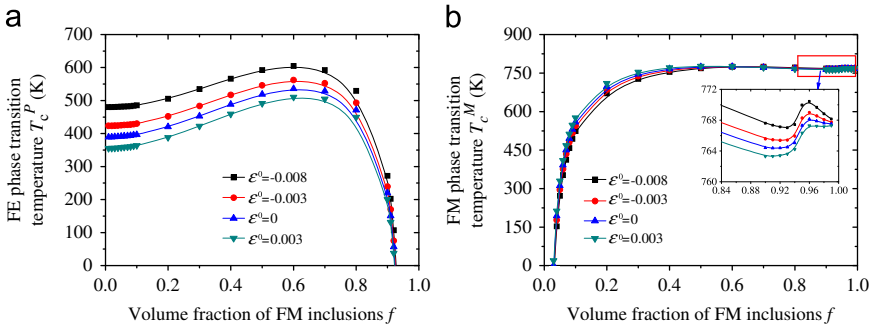

Fig. 1. Phase transition temperatures of (a) matrix $BaTiO_3$ and (b) inclusion $CoFe_2O_4$ vs. the volume fraction of ferromagnetic inclusions under different substrate strains. Inset in (b) is laid out for easy vision.

enhance the magnetization. For volume fraction less than about 50%, the vertical compressive strain applied to the $CoFe_2O_4$ pillars decreases with the increase of the substrate constraint due to the spontaneous polarization-induced stress relaxation, which can be clearly seen in the inset in Fig. 1(b). With further increase of the volume fractions, the relaxation of the spontaneous electrostriction becomes less important and the critical temperature increases with the increase of the in-plane constrain. The sharp decrease of FE phase transition temperature and increase of FM phase transition temperature were related with the surface and size effect. Since the Mori–Tanaka method cannot give exact prediction when the volume fraction is more than about 70%, our results just gave some hints about the surface and size effect even though the predicted values may be not exactly coincident with the experimental results.

As described above, the spontaneous polarization and magnetization are highly dependent on the temperature and the stress state in the heterostructures (Fig. 2). Since the lattice parameters of the FE phase, FM phase and the substrate are quite different, the stress states of each composite will vary with different volume fractions. With the decrease of the temperature and the increase of volume fraction of the FM inclusions, the polarization is enhanced with larger values than those of bulk counterparts. The magnetization is more complex because of the different stress state with respect to the volume fraction and the negative magnetostriction. The sharp decrease of the polarization and increase of magnetization were also related with the surface and size effect as happened in the phase transition temperatures.

The substrate-induced stress effect on the spontaneous polarization and magnetization is displayed in Fig. 3. Although magnetization and polarization can be greatly enhanced due to the misfit stress, the direct elastic interaction between the FE-induced eigenstrain and FM-induced eigenstrain is still week, which may be caused by the small magnetostriction and the clamping effect of the mismatch strain. As illustrated in the inset of Fig. 3(b), the pure magnetization-induced by the decrease of the polarization is relatively small because of the relative small magnetostriction of the $CoFe_2O_4$.

Further studies of the pure magnetization-induced polarization and pure polarization-induced magnetization are displayed in Fig. 4. The references of them are obtained by setting zero initial magnetization and zero polarization. The pure magnetization-induced polarization and pure polarization-induced magnetization were derived by comparing the real ones with the references. The magnitude of the induced polarization is three magnitude order lower than the bulk value. The polarization-induced magnetization is even worse and only several percent of the saturated magnetization. Because of the complex stress state with the interplay of the polarization, the induced magnetization showed inverse trend with respect to the temperature.

Physical properties versus the temperature of the FE phase such as the polarization, dielectric, and piezoelectric properties were shown in Fig. 5. The polarization decreased to zero when the temperature was cooled down below the phase transition temperature. The dielectric susceptibility versus temperature showed typical Curie–Wiess relationship and the unstable areas were around the critical points as shown in Fig. 5(b). The piezoelectric properties were also displayed and the results were in broad agreement with the experimental results available.

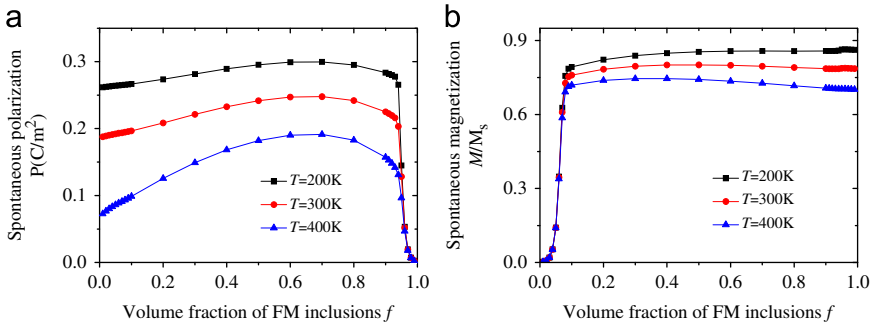

Fig. 2. (a) Spontaneous polarization and (b) relative spontaneous magnetization vs. the volume fraction of ferromagnetic inclusions under different temperatures.

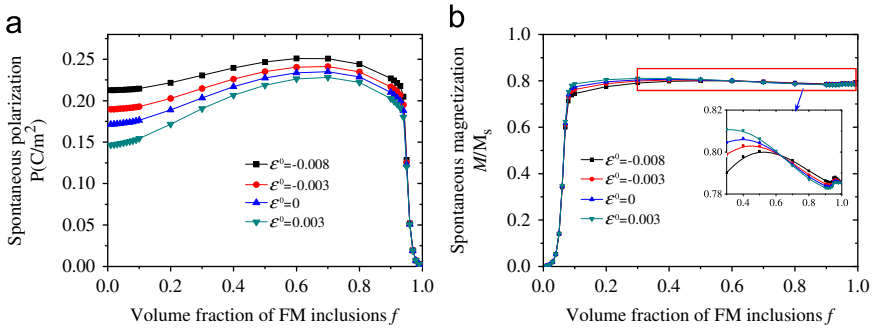

Fig. 3. (a) Spontaneous polarization and (b) relative spontaneous magnetization vs. the volume fraction of ferromagnetic inclusions under different substrate strains. Inset in (b) is laid out for easy vision.

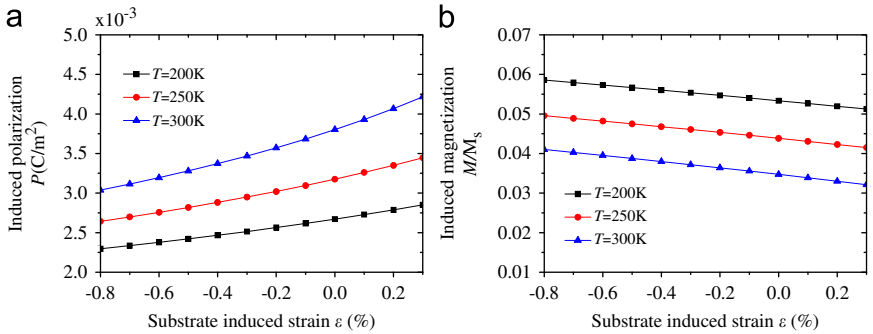

Fig. 4. (a) Induced magnetization and (b) induced polarization vs. substrate-induced strain under different temperatures.

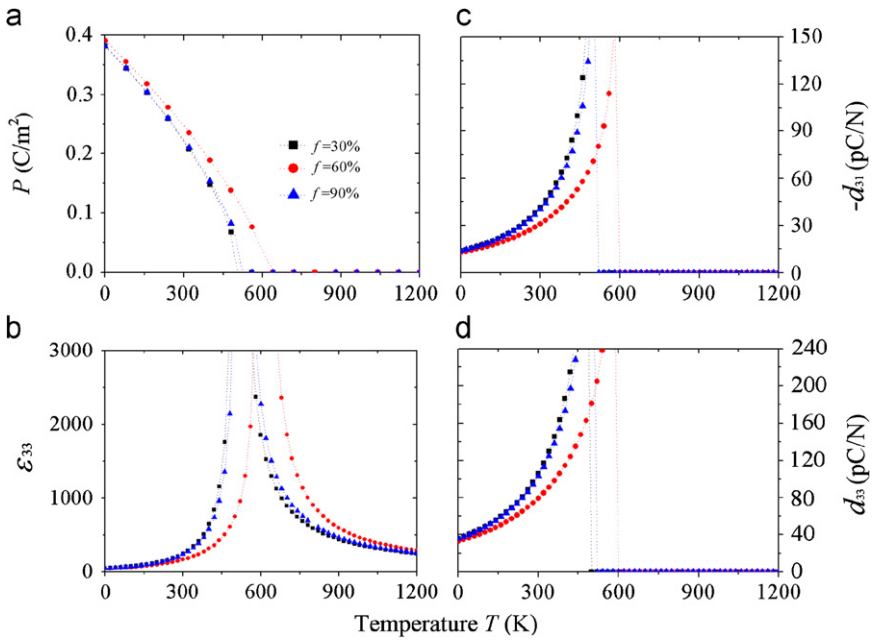

Fig. 5. Physical properties of the matrix $BaTiO_3$ vs. temperature with different volume fractions of ferromagnetic phase: (a) spontaneous polarization, (b) normalized dielectric susceptibility, (c) piezoelectric coefficient $-d_{31}$, and (d) piezoelectric coefficient d_{33}.

Magnetic properties of the FM phase, which were calculated in the similar way are displayed in Fig. 6. The relative susceptibility and the piezomagnetic coefficient of the materials in such a heterostructure were much smaller than those given for bulk materials in some literatures, such as the relative susceptibility $\mu/\mu_0$was set as 2 (Bichurin et al., 2003) and 125.6 (Li, 2000); the piezomagnetic coefficient q_{33} was 1885 (Liu et al., 2006) and 699.7 (Li, 2000). Besides the difference of the single crystal and polycrystalline, the pre-stress on the materials in such a highly strained structure may be the main cause of the discrepancy.

Using the modified parameters, the longitudinal ME coupling effect can be numerically calculated by using Eq. (31). As expected, the ME coupling coefficient is temperature dependent and increases with the decrease in temperature (Fig. 7(a)). In the room temperature, the maximum value of ME voltage coupling coefficients were slightly different with the change of the substrate strain (Fig. 7(b)). The maximum value was about 0.04 V/cmOe, which was much lower than most theoretical predictions based on the constitutive theory. The main difference may be caused by the small piezomagnetic coefficients calculated in this work. The ME coupling coefficient was unstable in the vicinity of the critical point and became to be zero below the critical thickness. This is quite a coincidence with the physical properties of the typical FE and FM nano-materials.

5. Summaries and conclusions

By using thermodynamic theory combined with the equivalent inclusion theory, a phenomenological model was constructed to study the ME coupling effect and the physical properties of nano-structured multiferroic composites.

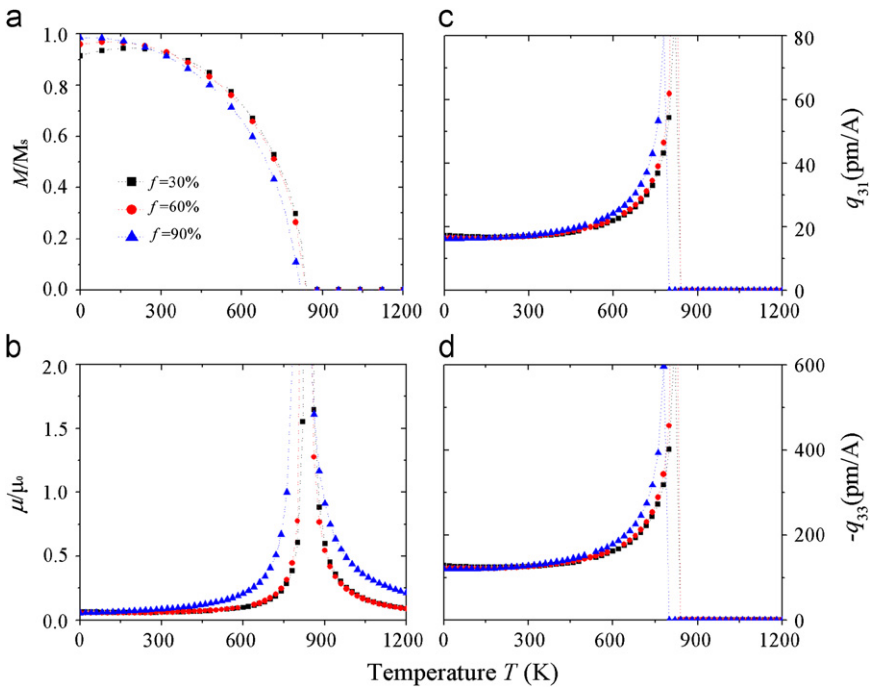

Fig. 6. Physical properties of the matrix $CoFe_2O_4$ vs. temperature with different volume fractions of ferromagnetic phase: (a) relative spontaneous magnetization, (b) permeability, (c) piezomagnetic coefficient p_{31}, and piezomagnetic coefficient p_{33}.

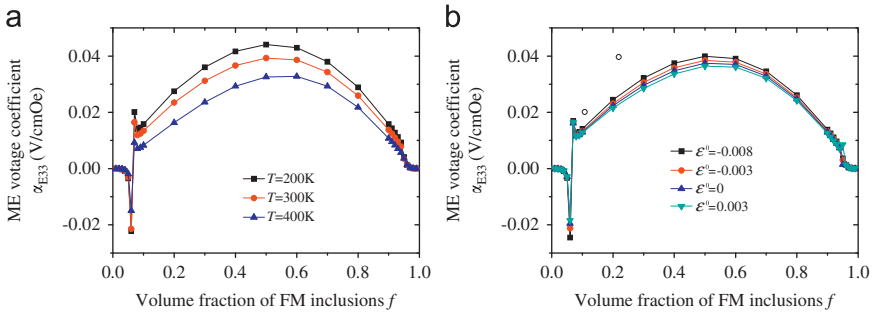

Fig. 7. Magnetoelectric voltage coefficients α_{33} vs. the volume fraction (a) under different temperatures and (b) under different substrate stains. Experimental data (open circles) in (b) taken from Liu et al. (2006) were also added for comparison.

The spontaneous polarization and magnetization were highly dependent on the temperature and substrate stain. Critical size existed in both the FE and FM phases. Magnetoelectric coupling coefficient was unstable in the vicinity of the critical size and disappeared below the critical size. Our theoretical approach predicted general trends and agreed in good quantitative with the experimental data. Base on the results, well matched heterostructures made up of materials with comparable magnetostriction and electrostriction were suggested for large ME coupling effect.

Acknowledgments

This project was supported by the National Science Foundation of China (Nos. 90815022 and 11002044), and the China Postdoctoral Science Foundation (No. 20090460068).

Appendix A

For cubic crystal with cylindrical shape and a circular cross-section the Eshelby tensor can be calculated by using the follow formulation for spheroid ($a_1=a_2$, $a_1/a_3=\rho$) with $\rho=0$:

$$S_{ijnm}=\frac{1}{8\pi}C_{pqnm}(\overline{G}_{ipiq}+\overline{G}_{jpiq}), \tag{A.1}$$

$$\overline{G}_{1111}=\overline{G}_{2222}=\frac{2\pi}{a}\int_0^1\frac{1-x^2}{pq}(1-x^2+\rho^2x^2)\left[\mu^2(1-x^2+\rho^2x^2)+\beta\rho^2x^2\right]dx+\frac{\pi}{a}\int_0^1\frac{(1-x^2)^2}{p(p+q)}\left[\beta(1-x^2+\rho^2x^2)+\gamma\rho^2x^2\right]dx, \tag{A.2a}$$

$$\overline{G}_{3333}=\frac{4\pi}{a}\int_0^1\frac{\rho^2x^2}{pq}(1-x^2+\rho^2x^2)\left[\mu^2(1-x^2+\rho^2x^2)+\beta(1-x^2)\right]dx+\frac{\pi\gamma}{a}\int_0^1\frac{\rho^2x^2(1-x^2)^2}{p(p+q)}dx, \tag{A.2b}$$

$$\overline{G}_{1122}=\overline{G}_{2211}=\frac{2\pi}{a}\int_0^1\frac{(1-x^2)}{pq}\left\{(1-x^2+\rho^2x^2)\left[\mu^2(1-x^2+\rho^2x^2)+\beta\rho^2x^2\right]+\left[\gamma\rho^2x^2+(1-x^2)\left[\beta(1-x^2+\rho^2x^2)\right]\right\}dx-\frac{\pi}{a}\int_0^1\frac{(1-x^2)^2}{p(p+q)}\left[\beta(1-x^2+\rho^2x^2)+\gamma\rho^2x^2\right]dx, \tag{A.2c}$$

$$\overline{G}_{1133}=\overline{G}_{2233}=\frac{2\pi}{a}\int_0^1\frac{\rho^2x^2}{pq}\left\{2(1-x^2+\rho^2x^2)\left[\mu^2(1-x^2+\rho^2x^2)+\beta\rho^2x^2\right]+(1-x^2)\left[\beta(1-x^2+\rho^2x^2)+\gamma\rho^2x^2\right]\right\}dx, \tag{A.2d}$$

$$\overline{G}_{1212}=-\frac{\pi(\lambda+\mu)}{a}\int_0^1\frac{(1-x^2)^2}{p(p+q)}\left[\mu(1-x^2+\rho^2x^2)+\mu'\rho^2x^2\right]dx, \tag{A.2e}$$

$$\overline{G}_{1313}=\overline{G}_{2323}=-\frac{2\pi\mu(\lambda+\mu)}{a}\int_0^1\frac{\rho^2x^2(1-x^2)(1-x^2+\rho^2x^2)}{pq}dx-\frac{\pi\mu'(\lambda+\mu)}{a}\int_0^1\frac{\rho^2x^2(1-x^2)^2}{p(p+q)}dx, \tag{A.2f}$$

$$\overline{G}_{3311}=\overline{G}_{3322}=\frac{2\pi}{a}\int_0^1\frac{(1-x^2)}{pq}(1-x^2+\rho^2x^2)\left[\mu^2(1-x^2+\rho^2x^2)+\beta(1-x^2)\right]dx+\frac{\pi\gamma}{2a}\int_0^1\frac{(1-x^2)^3}{p(p+q)}dx, \tag{A.2g}$$

where

$$\rho=a_1/a_3,$$
$$a=\mu^2(\lambda+2\mu+\mu'),$$
$$b=a^{-1}\mu\mu'(2\lambda+2\mu+\mu'),$$
$$c=a^{-1}\mu'^2(3\lambda+3\mu+\mu'),$$
$$\beta=\mu(\lambda+2\mu+\mu'),$$
$$\gamma=\mu'(2\lambda+2\mu+\mu'),$$
$$p=\left\{(1-x^2+\rho^2x^2)^3+b\rho^2x^2(1-x^2)(1-x^2+\rho^2x^2)+\tfrac{1}{4}(1-x^2)^2\left[b(1-x^2+\rho^2x^2)+c\rho^2x^2\right]\right\}^{1/2},0<x<1,$$
$$q=\left\{(1-x^2+\rho^2x^2)^3+b\rho^2x^2(1-x^2)(1-x^2+\rho^2x^2)\right\}^{1/2}\quad 0<x<1.$$

References

Benveniste, Y., 1987. A new approach to the application of Mori–Tanaka theory in composite-materials. Mech. Mater. 6, 147.

Benveniste, Y., 1995. Magnetoelectric effect in fibrous composites with piezoelectric and piezomagnetic phases. Phys. Rev. B 51, 16424.

Bichurin, M., Petrov, V., Srinivasan, G., 2003. Theory of low-frequency magnetoelectric coupling in magnetostrictive–piezoelectric bilayers. Phys. Rev. B 68, 54402.

Bratkovsky, A., Levanyuk, A., 2005. Smearing of phase transition due to a surface effect or a bulk inhomogeneity in ferroelectric nanostructures. Phys. Rev. Lett. 94, 107601.

Brintlinger, T., Lim, S., Baloch, K., Alexander, P., Qi, Y., Barry, J., Melngailis, J., Salamanca-Riba, L., Takeuchi, I., Cumings, J., 2010. In situ observation of reversible nanomagnetic switching induced by electric fields. Nano Lett. 10, 1219.

Brown, G., Novotny, M., Rikvold, P., 2001. Langevin simulation of thermally activated magnetization reversal in nanoscale pillars. Phys. Rev. B 64, 134422.

Chambers, S., Farrow, R., Maat, S., Toney, M., Folks, L., Catalano, J., Trainor, T., Brown, G., 2002. Molecular beam epitaxial growth and properties of $CoFe_2O_4$ on MgO (0 0 1). J. Magn. Magn. Mater. 246, 124.

Cottam, M., Tilley, D., Zeks, B., 1984. Theory of surface modes in ferroelectrics. J. Phys. C: Solid State Phys. 17, 1793.

Eshelby, J., 1957. The determination of the elastic field of an ellipsoidal inclusion, and related problems. Proc. R. Soc. London: Ser. A, 376.

Garcia, V., Bibes, M., Bocher, L., Valencia, S., Kronast, F., Crassous, A., Moya, X., Enouz-Vedrenne, S., Gloter, A., Imhoff, D., 2010. Ferroelectric control of spin polarization. Science 327, 1106.

Harshe, G., Dougherty, J., Newnham, R., 1993a. Theoretical modeling of 3-0/0-3 magnetoelectric composites. Int. J. Appl. Electromagn. Mater. 4, 161.

Harshe, G., Dougherty, J., Newnham, R., 1993b. Theoretical modeling of multilayer magnetoelectric composites. Int. J. Appl. Electromagn. Mater. 4, 145.

Huang, G., Wang, B., Mai, Y., 2009. Effective properties of magnetoelectroelastic materials with aligned ellipsoidal voids. Mech. Res. Commun. 36, 563.

Li, J., 2000. Magnetoelectroelastic multi-inclusion and inhomogeneity problems and their applications in composite materials. Int. J. Eng. Sci. 38, 1993.

Li, J., Dunn, M., 1998. Micromechanics of magnetoelectroelastic composite materials: average fields and effective behavior. J. Intell. Mater. Syst. Struct. 9, 404.

Liu, G., Nan, C., Sun, J., 2006. Coupling interaction in nanostructured piezoelectric/magnetostrictive multiferroic complex films. Acta Mater. 54, 917.

Lou, J., Liu, M., Reed, D., Ren, Y., Sun, N., 2009. Giant electric field tuning of magnetism in novel multiferroic Fegab/Lead Zinc Niobate-Lead Titanate (PZN-PT) heterostructures. Adv. Mater. 21, 4711.

Lu, X., Wang, B., Zheng, Y., Ryba, E., 2007. Coupling interaction in 1-3-type multiferroic composite thin films. Appl. Phys. Lett. 90, 133124.

Lu, X., Wang, B., Zheng, Y., Ryba, E., 2009. Phenomenological theory of 1–3 type multiferroic composite thin film: thickness effect. J. Phys. D. Appl. Phys. 42, 015309.

MacManus-Driscoll, J., Zerrer, P., Wang, H., Yang, H., Yoon, J., Fouchet, A., Yu, R., Blamire, M., Jia, Q., 2008. Strain control and spontaneous phase ordering in vertical nanocomposite heteroepitaxial thin films. Nature Mater. 7, 314.

Martin, L.W., Chu, Y.H., Ramesh, R., 2010. Advances in the growth and characterization of magnetic, ferroelectric, and multiferroic oxide thin films. Mater. Sci. Eng. R: Rep. 68, 89.
Mori, T., Tanaka, K., 1973. Average stress in matrix and average elastic energy of materials with misfitting inclusions. Acta Metall. 21, 571.
Mura, T., 1987. Micromechanics of Defects in Solids, 2nd ed. Martinus Nijhoff, Dordrecht.
Nan, C., 1994. Magnetoelectric effect in composites of piezoelectric and piezomagnetic phases. Phys. Rev. B 50, 6082.
Nan, C.W., Bichurin, M.I., Dong, S.X., Viehland, D., Srinivasan, G., 2008. Multiferroic magnetoelectric composites: historical perspective, status, and future directions. J. Appl. Phys. 103, 031101.
Nelson, C., Rzchowski, M., Pan, X., Ramesh, R., Chen, L., Eom, C., 2010. Ferroelastic switching for nanoscale non-volatile magnetoelectric devices. Nature Mater. 3, 309.
Ni, Y., He, L., Khachaturyan, A.G., 2010. Equivalency principle for magnetoelectroelastic multiferroics with arbitrary microstructure: the phase field approach. J. Appl. Phys. 108, 023504.
Qu, B., Zhong, W., Prince, R., 1997. Interfacial coupling in ferroelectric superlattices. Phys. Rev. B 55, 11218.
Slutsker, J., Tan, Z., Roytburd, A., Levin, I., 2007. Thermodynamic aspects of epitaxial self-assembly and magnetoelectric response in multiferroic nanostructures. J. Mater. Res. 22, 2088.
Wang, B., Woo, C., 2008. Magnetoelectric effects due to elastic coupling in ferroelectric/ferromagnetic multilayers. J. Appl. Phys. 103, 124107.
Wang, B., Woo, C., 2009. Curie temperature and critical thickness of ferroelectric thin films. J. Appl. Phys. 97, 084109.
Woo, C., Zheng, Y., 2008. Depolarization in modeling nano-scale ferroelectrics using the Landau free energy functional. Appl. Phys. A: Mater. 91, 59.
Wu, P.P., Ma, X.Q., Zhang, J.X., Chen, L.Q., 2010. Phase-field model of multiferroic composites: domain structures of ferroelectric particles embedded in a ferromagnetic matrix. Philos. Mag. 90, 125.
Zavaliche, F., Zhao, T., Zheng, H., Straub, F., Cruz, M., Yang, P., Hao, D., Ramesh, R., 2007. Electrically assisted magnetic recording in multiferroic nanostructures. Nano Lett. 7, 1586.
Zhang, J., Li, Y., Schlom, D., Chen, L., Zavaliche, F., Ramesh, R., Jia, Q., 2007a. Phase-field model for epitaxial ferroelectric and magnetic nanocomposite thin films. Appl. Phys. Lett. 90, 052909.
Zhang, J.X., Li, Y.L., Schlom, D.G., Chen, L.Q., Zavaliche, F., Ramesh, R., Jia, Q.X., 2007b. Phase-field model for epitaxial ferroelectric and magnetic nanocomposite thin films. Appl. Phys. Lett. 90, 052909.
Zheng, H., Wang, J., Lofland, S., Ma, Z., Mohaddes-Ardabili, L., Zhao, T., Salamanca-Riba, L., Shinde, S., Ogale, S., Bai, F., 2004. Multiferroic $BaTiO_3$-$CoFe_2O_4$ nanostructures. Science 303, 661.
Zheng, Y., Cai, M., Woo, C., 2010. Critical properties of symmetric nanoscale metal-ferroelectric-metal capacitors. Acta Mater. 58, 3050.